This article has been accepted for publication in a future issue of this journal, but has not been fully edited. Content may change prior to final publication. Citation information: DOI 10.1109/TPWRD.2018.2816813, IEEE Transactions on Power Delivery

A Fully Decentralized Control of Grid-Connected Cascaded Inverters

Xiaochao Hou, *Student Member, IEEE*, Yao Sun, *Member, IEEE*, Hua Han, Zhangjie Liu, Wenbin Yuan and Mei Su

[1]***Abstract*—This letter proposes a decentralized power balance control for grid-connected cascaded modular inverters without any communication, and each module makes decisions based on its own local information. In contrast, the conventional methods are usually centralized control and depend on a real-time communication. Thus, the proposed scheme has advantages of improved reliability and decreased costs. The overall system stability is analyzed, and the stability condition is derived as well. The feasibility of the proposed method is verified by simulation.**

***Index Terms*—Cascaded inverters, Decentralized control, Grid-connected mode, Power balance, Renewable generation;**

I. Introduction

Multiple inverters are widely connected in parallel-type to form a high power rating power network [1] or cascaded-type manners to form a high voltage level power network [2]. These cascaded-type inverters are early applied to multilevel topologies [3], and extended into distributed generations, especially for PV grid-connected system [4], micro-grids [5] and battery balance managements [6]. Most power balance methods of cascaded-type system are centralized with high bandwidth communications in grid-connected mode, which severely limits its application scope [3]-[6]. For cascaded micro-converters, [7] firstly proposes a novel power balance control with low bandwidth communications. The central controller of string converters interconnects the local controllers of micro-converters by transferring slow dynamic DC components. Though excellent power balance and voltage quality are achieved, they do not go beyond a communication-based category [3]-[7].

Cascaded inverters have distinct merits in grid-connected mode, but the power balance among all modules has not been researched in decentralized manners. In this letter, we introduce a *P-* ω droop control for frequency synchronization and power balance autonomously. The stability of the proposed scheme is proved in theory and the effectiveness is verified by simulation results.

II. Analysis of Decentralized Power Balance Control

A. Equivalent Models of Grid-Connected Cascaded Inverters

Fig. 1 illustrates the schematic diagram of grid-connected cascaded-type inverters. This configuration is beneficial to integrate low-voltage DC distributed generations (DGs) into medium voltage system. It is very common in PV grid-connected applications.

From Fig.1, the output real power P_i and reactive power Q_i of *i-th* module are derived as follows

$$P_i + jQ_i = V_i e^{j\delta_i} \cdot \left((V_p e^{j\delta_p} - V_g e^{j\delta_g}) / (|Z_{line}| e^{j\theta_{line}}) \right)^* \quad (1)$$

where V_i and δ_i represent the output voltage amplitude and phase angle of *i-th* module. V_g and δ_g are the voltage amplitude and phase angle of utility grid. $|Z_{line}|$ and θ_{line} are the grid impedance amplitude and angle. Usually, the grid impedance is mainly inductive ($\theta_{line} \approx \pi/2$). The voltage $V_p e^{j\delta_p}$ at point of common coupling (PCC) is the sum of each module voltage.

$$V_p e^{j\delta_p} = \sum_{j=1}^{N} V_j e^{j\delta_j} \quad (2)$$

where N represents the total number of cascaded modules.

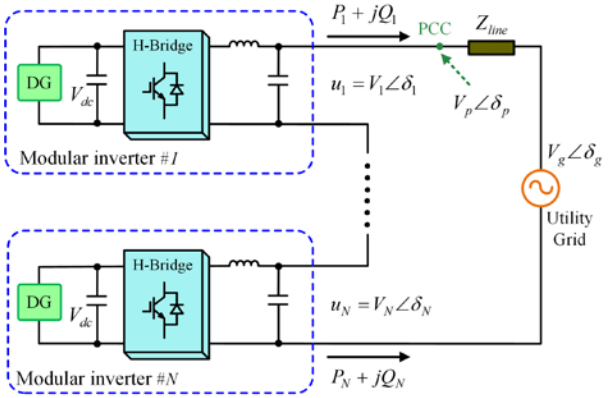

Fig. 1. Schematic diagram of grid-connected cascaded-type inverters.

From (1)-(2), the power transmission characteristic is given

$$P_i = \frac{V_i}{|Z_{line}|} \left(V_g \sin(\delta_i - \delta_g) - \sum_{j=1}^{N} V_j \sin(\delta_i - \delta_j) \right) \quad (3)$$

$$Q_i = \frac{V_i}{|Z_{line}|} \left(\sum_{j=1}^{N} V_j \cos(\delta_i - \delta_j) - V_g \cos(\delta_i - \delta_g) \right) \quad (4)$$

B. Proposed P- ω Droop Control

To synchronize each module with the grid and realize power balance without communication, a decentralized control scheme is designed as

$$\omega_i = \omega^* - k \cdot (P_i - P^*) \quad (5)$$

$$V_i = V^* = V_g / M \quad (6)$$

where ω_i and V_i are the angular frequency and voltage amplitude references of *i-th* module, respectively. ω^* represents the nominal value of the grid angular frequency. P^*

[1] Manuscript received September 10, 2017; revised December 3, 2017; accepted February 26, 2018. This work was supported in part by the National Natural Science Foundation of China under Grants 61622311 and 61573384, in part by the Joint Research Fund of Chinese Ministry of Education under Grant 6141A020335, and in part by the Hunan Provincial Innovation Foundation for Postgraduate. *(Corresponding author: Yao Sun.)*

X. Hou, Y. Sun, H. Han, Z. Liu, W. Yuan and M. Su are with the School of Information Science and Engineering, Central South University, Changsha 410083, China (e-mail: houxc10@csu.edu.cn; yaosuncsu@gmail.com; hua_han@126.com; 956142207@qq.com; ywb_csu@163.com; sumeicsu@csu.edu.cn).

This article has been accepted for publication in a future issue of this journal, but has not been fully edited. Content may change prior to final publication. Citation information: DOI 10.1109/TPWRD.2018.2816813, IEEE Transactions on Power Delivery

represents the nominal rated power of each module. k is a positive coefficient of P-ω droop control. M is a critical parameter related with stability, which is designed later.

C. Steady-State Analysis

In steady state, because the voltage amplitude reference V^* is same for all modules and each module shares the same grid current, the apparent power of each module is equal. Moreover, (7) is obtained due to the identical grid frequency from (5)

$$P_1 = P_2 = \cdots = P_N = P^* \tag{7}$$

Namely, the phase angles of all modules are equal in steady state (δ_i=δ_j; $i, j \in \{1,2\ldots N\}$). Thus, the voltage amplitude and phase angle of PCC is derived from (2)

$$V_p = NV^* = (N/M)\cdot V_g; \qquad \delta_p = \delta_1 = \delta_2 = \cdots = \delta_N \tag{8}$$

Then, the steady state power of each module is obtained from (3)-(6)

$$P^* = S_C \sin\bar{\delta}; \quad \bar{Q}_i = S_C\left(N/M - \cos\bar{\delta}\right) \tag{9}$$

where $S_C = V_g^2/(M\cdot|Z_{line}|)$ represents the power transfer capacity of a single module. $\bar{\delta} = \delta_p - \delta_g$ is referred to as the steady power angle. From (9), there are two steady points and they are $\bar{\delta} = \arcsin(\frac{P^*}{S_C})$ or $\bar{\delta} = \pi - \arcsin(\frac{P^*}{S_C})$.

D. Stability Analysis

In this section, the small signal analysis is carried out to test the system stability. Since $\dot{\delta}_i = \omega_i$, combining (3)-(6) and linearizing them around the steady state points yield

$$\dot{\tilde{\delta}}_i = -k'\left(M(\cos\bar{\delta})\left(\tilde{\delta}_i - \tilde{\delta}_g\right) - \sum_{j=1, j\neq i}^{N}\left(\tilde{\delta}_i - \tilde{\delta}_j\right)\right) \tag{10}$$

where $k' = kV^{*2}/|Z_{line}|$, and $\tilde{\delta}_i$, $\tilde{\delta}_g$, $\tilde{\delta}_j$ denote small perturbations around the equilibrium point.

Rewrite (10) in matrix form as

$$\dot{\tilde{\delta}} = -k'\cdot L\cdot\tilde{\delta} \tag{11}$$

where $\tilde{\delta} = \begin{bmatrix}\tilde{\delta}_1 & \tilde{\delta}_2 & \cdots & \tilde{\delta}_N\end{bmatrix}^T$;

$$L = \begin{bmatrix} M\cos\bar{\delta} - N + 1 & 1 & \cdots & 1 \\ 1 & M\cos\bar{\delta} - N + 1 & \cdots & 1 \\ \vdots & \vdots & \ddots & \vdots \\ 1 & 1 & \cdots & M\cos\bar{\delta} - N + 1 \end{bmatrix} = (M\cos\bar{\delta} - N)I_{N\times N} + 1_N 1_N^T$$

The eigenvalues of the system matrix $A = -k'L$ are given by

$$\lambda_1(A) = -k'M\cos\bar{\delta}; \quad \lambda_2(A) = \cdots = \lambda_N(A) = -k'(M\cos\bar{\delta} - N). \tag{12}$$

Thus, the necessary and sufficient condition of system stability is obtained as follow

$$\Delta = M\cos\bar{\delta} - N > 0 \tag{13}$$

From (13), since both M and N are greater than zero, the power angle $\bar{\delta}$ should lie in (-π/2, π/2) under the stability constraint. According to the above steady-state analysis, only $\bar{\delta} = \arcsin(P^*/S_C)$ is a stable equilibrium point in (13). From (9), to obtain a high power factor, Δ should be as small as possible. However, a too small Δ is detrimental to stability from (12). Thus, a proper M should be designed by making a tradeoff between reactive power requirement and stability margin.

III. Simulation Results

The simulation tests are carried out to validate the proposed ideas. The control block diagram of *i-th* module is presented in Fig. 2. The proposed control algorithm in (5)-(6) is used to generate the voltage reference for the inner voltage-current closed-loops. The simulation parameters of the system are listed in Table I.

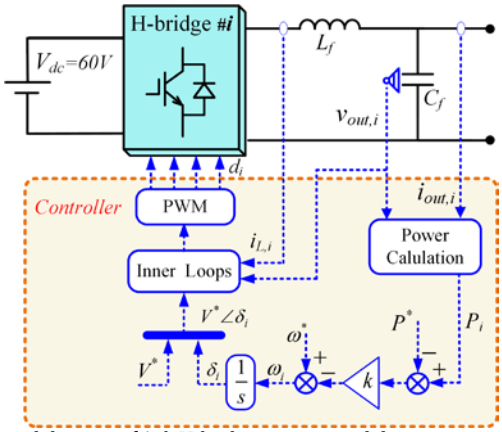

Fig. 2. Control diagram of *i-th* H-bridge inverter module.

TABLE I
SIMULATION PARAMETERS

Symbol	Value	Symbol	Value
V_g	311 V		**5.8** (case-1)
ω^*	2π*50 rad/s	M	**6.2** (case-2)
P^*	4 kW		**7.0** (case-3)
k	1.2e-3		**53.6** V (case-1)
Z_{line}	0.1+j0.5 Ω	V^*	**50.1** V (case-2)
N	6		**44.4** V (case-3)

Based on the steady-state analysis (9) and stability condition (13), three cases of different M are discussed.

Fig.3 shows the simulation results in case-1. Since $M < N$, the stability condition of (13) is not met, thus the system is unstable and the output real-power/reactive-power of modules are unbalanced.

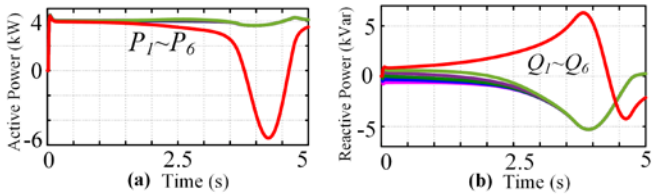

Fig. 3. Simulation results of case-1. (a) Active power, (b) reactive power.

In case-2, as the selected M satisfies the stability condition (13), the system works normally. The simulation results are illustrated in Fig. 4. As seen from Fig. 4(a)-(b), real-power/reactive-power balance is achieved. Fig. 4(c) indicates that the frequency synchronization is also obtained. Fig.4 (d) shows the voltage/current waveforms at PCC.

Fig. 5(a)-(d) show simulation results of case-3. Compared with case-2, the settling time becomes shorter, but the power factor becomes lower from 0.983 to 0.891 in Fig. 6(a). Therefore, in practice, M is designed by making a compromise between the power factor and dynamic response. In addition, Fig. 6(b) shows that the steady-state power angles of case-2 and case-3 lie in (-π/2, π/2), which is in accordance with the former stability analysis.

This article has been accepted for publication in a future issue of this journal, but has not been fully edited. Content may change prior to final publication. Citation information: DOI 10.1109/TPWRD.2018.2816813, IEEE Transactions on Power Delivery

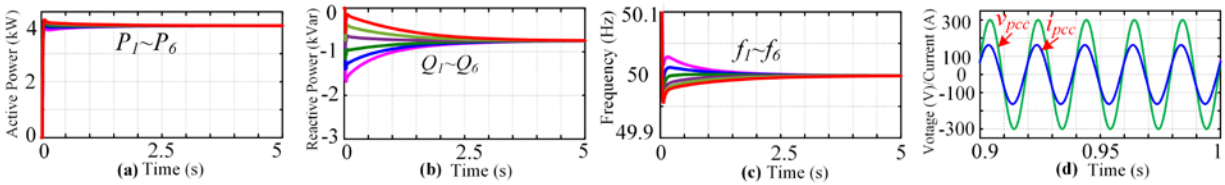

Fig. 4. Simulation results of case-2. (a) Active power, (b) reactive power, (c) frequency, (d) voltage/current at PCC.

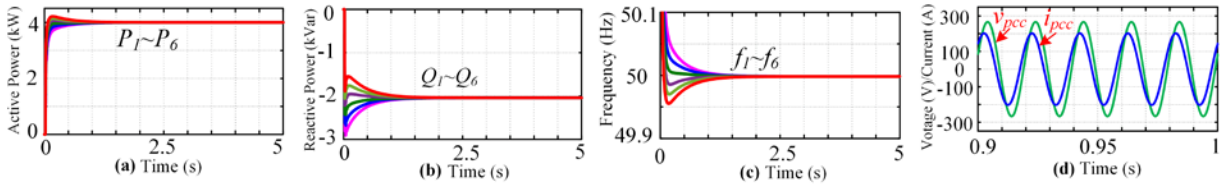

Fig. 5. Simulation results of case-3. (a) Active power, (b) reactive power, (c) frequency, (d) voltage/current at PCC.

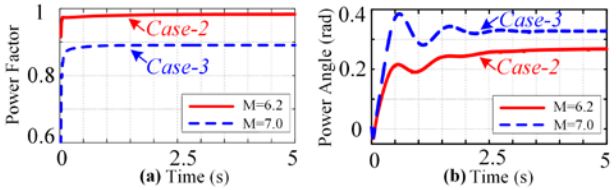

Fig. 6. Comparison of case-2 and case-3. (a) Power factor, (b) power angle.

IV. Conclusion

As an important supplementary, this letter presents a fully decentralized control for cascaded inverter system in grid-connected mode. It realizes accurate power balance and frequency synchronization autonomously without relying on any communication. Based on this fundamental study, some novel hierarchical control schemes would be constructed for future PV and storage cascaded systems, where decentralized control takes a role of primary control. For readers, this letter explores the possibilities of inspiring new methods in a hybrid power network with cascaded-type and parallel-type inverters.

V. References

[1] Y. Sun, X. Hou, J. Yang, H. Han, M. Su, and J. M. Guerrero, "New perspectives on droop control in AC microgrid," *IEEE Transactions on Ind. Electron.*, vol. 64, no. 7, pp. 5741-5745, Jul. 2017.

[2] Y. Sun, G. Shi, X. Li, W. Yuan, M. Su, H. Han, and X. Hou, "An f-P/Q droop control in cascaded-type microgrid," *IEEE Transactions on Power Systems*, vol. 33, no. 1, pp. 1136-1138, Jan. 2018.

[3] M. Malinowski, K. Gopakumar, J. Rodriguez, and M. P´erez, "A survey on cascaded multilevel inverters," *IEEE Trans. Ind. Electron.*, vol. 57, no. 7, pp. 2197–2206, Jul. 2010.

[4] Y. Yu, G. Konstantinou, B. Hredzak, and V. G. Agelidis, "Power balance of cascaded H-bridge multilevel converters for large-scale photovoltaic grid integration," *IEEE Trans. Power Electron.*, vol. 31, no. 1, pp. 292–303, Jan. 2016.

[5] A. Mortezaei, M. G. Simoes, A.S. Bubshait, T.D.C. Busarello, F.P. Marafao, and A. Al-Durra, "Multifunctional control strategy for asymmetrical cascaded H-bridge inverter in microgrid applications," *IEEE Trans. Ind. Appl.*, pp. 1–14, Nov. 2016.

[6] E. Chatzinikolaou and D. J. Rogers, "A comparison of grid-connected battery energy storage system designs," *IEEE Trans. Power Electron.*, vol. 32, no. 9, pp. 6913-6923, Sep. 2017.

[7] J. He, Y.W. Li, C. Wang, Y. Pan, C. Zhang, and X. Xing, "A hybrid microgrid with parallel and series connected micro-converters," *IEEE Trans. Power Electron.*, vol. 33, no. 6, pp. 4817-4831, Jun. 2018.